



# Influence of $Zr^{4+}$ ions on solar absorbance and emissivity of coatings formed on AZ31 Mg alloy by plasma electrolytic oxidation



Hang Li<sup>a</sup>, Songtao Lu<sup>a</sup>, Xiaohong Wu<sup>a,\*</sup>, Wei Qin<sup>b,\*</sup>

<sup>a</sup> Department of Chemistry, Harbin Institute of Technology, Harbin, Heilongjiang 150001, PR China

<sup>b</sup> School of Materials Science and Engineering, Harbin Institute of Technology, Harbin, Heilongjiang 150001, PR China

## ARTICLE INFO

Available online 7 February 2015

### Keywords:

Mg alloy  
Plasma electrolytic oxidation  
Thermal control coating

## ABSTRACT

The thermal control coatings with low absorbance–emissivity ratio were successfully fabricated on AZ31 Mg alloy by plasma electrolytic oxidation (PEO) technique. The influence of  $Zr(NO_3)_4$  on the thermal control properties of the PEO coatings was studied in detail. The micro-structure, element distribution, phase and chemical composition of the prepared coatings were characterized by analytical techniques. The solar absorbance and emissivity of the coatings were respectively measured by a solar absorption/reflectorimeter and an ultraviolet–visible–near infrared spectrophotometer. The results revealed that the coatings were composed of MgO, t-ZrO<sub>2</sub> and an Mg–O–Zr compound ( $Mg_{0.13}Zr_{0.87}O_{1.87}$ ), as well as some non-crystalline phosphorus. The EDS results showed the existence of Mg, O, Zr, P, Na and K elements on the porous coating with different shapes and sizes. The thickness, roughness and thermal control properties of the coatings were greatly affected by the content of  $Zr^{4+}$  ions in the electrolyte. When the concentration was 10 g/L, the coating possessed the lowest absorbance–emissivity ratio (about 0.46) and the maximum thickness. Herein, the solar absorbance was 0.405 and the emissivity reached 0.873. The thermal control coating obtained by this method will broaden the spatial application of Mg alloy.

© 2015 Elsevier B.V. All rights reserved.

## 1. Introduction

Magnesium and its alloys have been gradually used as the attractive material option of the spacecraft for saving energy [1–3], owing to its excellent properties, such as low weight (about 1.83 g/cm<sup>3</sup>), good electromagnetic shielding property, and high specific strength and modulus [4–6]. However, the high intensity solar radiation in the space environment can raise the temperature of the spacecraft surface to levels that could cause temperature-sensitive apparatuses out-of operation [7–9]. Besides, the internal heat from the electron devices further makes the difficulty of the thermal controlling of the spacecraft [10,11]. Effective thermal prevention measures are in urgent need for ensuring the operating temperature of spacecraft. And a common passive method of thermal protection is thermal control coating, two performance parameters of which are the solar absorbance ( $\alpha_s$ ) and the emissivity ( $\varepsilon$ ) [12–14]. This is of great significance for preparing thermal control coating on magnesium alloys with low emissivity (about 0.08).

Due to the effect of vacuum environment, the convection and conduction of heat are not generated in space, and the only heat radiation is allowed [15–17]. The function of thermal control coatings is to provide a radiating pathway to achieve the purpose of the heat rejection. The equilibrium temperature of an object surface is mainly controlled

by regulating the  $\alpha_s/\varepsilon$  ratio of thermal control coatings as described by Eq. (1) [18]:

$$A_t \varepsilon T_o^4 = S \alpha_s A_e \quad (1)$$

where,  $A_t$  is the total area of an object surface,  $A_e$  is the area of the surface exposed to the sunlight,  $\sigma$  is the Stefan–Boltzmann constant,  $S$  is the solar constant, and  $T_o$  is the absolute temperature of an object. It is obvious that the ideal thermal control coating should have lower solar absorbance and higher emissivity, namely the minimum  $\alpha_s/\varepsilon$  ratio. Many preparation techniques about this coating have been developed, such as thermal spraying, physical vapor deposition, anodic oxidation, sol–gel and so on [19–23]. The coatings fabricated by the traditional anodizing oxidation on aluminum alloys are usually thin and easily resulted in the property degradation under the vacuum ultraviolet radiation, and the process of physical vapor deposition requires a rigorous vacuum environment. PEO is a novel technique to in-situ form ceramic coatings on Al, Mg, Ti and their alloys [24–26], which can acquire excellent properties, such as biocompatibility, corrosion and wear resistance [27–29]. This technique is developed based on anodic oxidation and yet distinguishes itself from conventional anodizing by using advanced high voltages above the dielectric breakdown potential [30,31]. The discharge and exothermic phenomena are important characteristics during the PEO process. The formation mechanism of the coating is complex due to the involvement of thermal diffusion, electro- and plasma-chemical reactions on the interface of the electrode [32,33]. Complicated ion

\* Corresponding authors. Tel.: +86 451 864 02522.

E-mail addresses: [wuxiaohong@hit.edu.cn](mailto:wuxiaohong@hit.edu.cn) (X. Wu), [qinwei@hit.edu.cn](mailto:qinwei@hit.edu.cn) (W. Qin).

transfer occurs on the liquid/gas, gas/solid, and solid/liquid interfaces [30]. The used electrolytes generally include silicate, phosphate, hydroxide and fluoride [34,35]. Moreover, the process is simply and conducted at room temperature. In our previous research, thermal control coatings with high  $\alpha_s$  and high  $\varepsilon$  have been prepared on AZ31 Mg alloy by the PEO method [36].

In this paper, the white thermal control coating with low  $\alpha_s/\varepsilon$  ratio was achieved on AZ31 Mg alloy usually used as the material of electronic packages. The coatings were prepared in the phosphate electrolyte containing  $Zr(NO_3)_4$  by the PEO technique. Our results indicate that the incorporation of Zr ion plays a great role on the microstructure, composition and thermal control properties of the obtained coatings. The solar absorbance and emissivity of the coating prepared at 10 g/L  $Zr(NO_3)_4$  were 0.405 and 0.873, respectively. These results demonstrate that such coatings are of great potential thermal control system in the spacecraft.

## 2. Experimental

### 2.1. Preparation of the PEO coatings

AZ31 magnesium alloys (Al 3–3.2%, Zn 0.8%, Mn 0.4%, Si 0.02%, Cu 0.003%, Fe 0.0023% and Mg balance) were purchased from local market (Northeast light alloy co., LTD.; Harbin) and employed in this work. Before PEO treatment, the square samples (dimension: 40 mm  $\times$  40 mm  $\times$  2 mm) were successively polished with 400, 1000, and 2000 grit waterproof abrasive papers, and then ultrasonically cleaned for 5 min in the acetone solution and followed by distilled water. The sample served as an anode, while a stainless steel electro-bath served as a cathode. A home-made bipolar pulse power of 20 kW was used for PEO process in the constant current mode and employed to prepare thermal control ceramic coatings on Mg alloy surface. The reaction temperature

was kept below 30 °C by the circulating system of cooling water. The electrolytes were consisted of  $Na_5P_3O_{10}$  (30 g/L), KOH (5 g/L), NaF (0.5 g/L) and  $Na_2EDTA$  (1 g/L), as well as the additive  $Zr(NO_3)_4$  with different concentrations (0 g/L, 5 g/L, 10 g/L, 15 g/L). All the PEO treatments were performed under the same technical parameters. The current density, frequency, duty ratio and oxidation time were kept at 10 A/dm<sup>2</sup>, 50 Hz, 45% and 15 min, respectively. Details of the PEO process were described by M. Boinet group [37]. After the PEO process, the coated samples were washed with distilled water and then dried in air.

### 2.2. Characterization of the PEO coatings

The surface and cross-sectional morphologies of the PEO coatings were characterized by a scanning electron microscope (SEM; Hitachi S-570) equipped with energy dispersive spectroscopy (EDS). The 3D surface structure of the prepared coating was measured by a CSPM 5500 scanning probe microscope system (Being Nano-Instruments co., LTD; Beijing) and the Root Mean Square (rms) surface roughness was obtained. Meanwhile the relative content and distribution of elements on the coating surface were investigated. Crystal structure was examined by X-ray diffraction (XRD; Dmax-3B, Rigaku, Japan) with a Cu-K $\alpha$  radiation. Components and chemical states of the coating were evaluated by using an X-ray photoelectron spectroscopy (XPS; Escalab-220IXL, VG Scientific Ltd, UK) with a typically Al-K $\alpha$  radiation. The bonding strengths of the obtained coatings were measured by the pull-off method using an electronic universal testing machine (WDW-100, Heng Rui Jin Testing Machine co., LTD.; China). A PEO treated sample was adhered to the bare AZ31 alloy sample using an epoxy resin (E-7 type) produced in Shanghai Research Institute of Synthetic Resins. And the epoxy was cured at 100 °C for 3 h. All tests were carried out at a stretching rate of 0.2 mm/min and based on ISO 14916 [38].

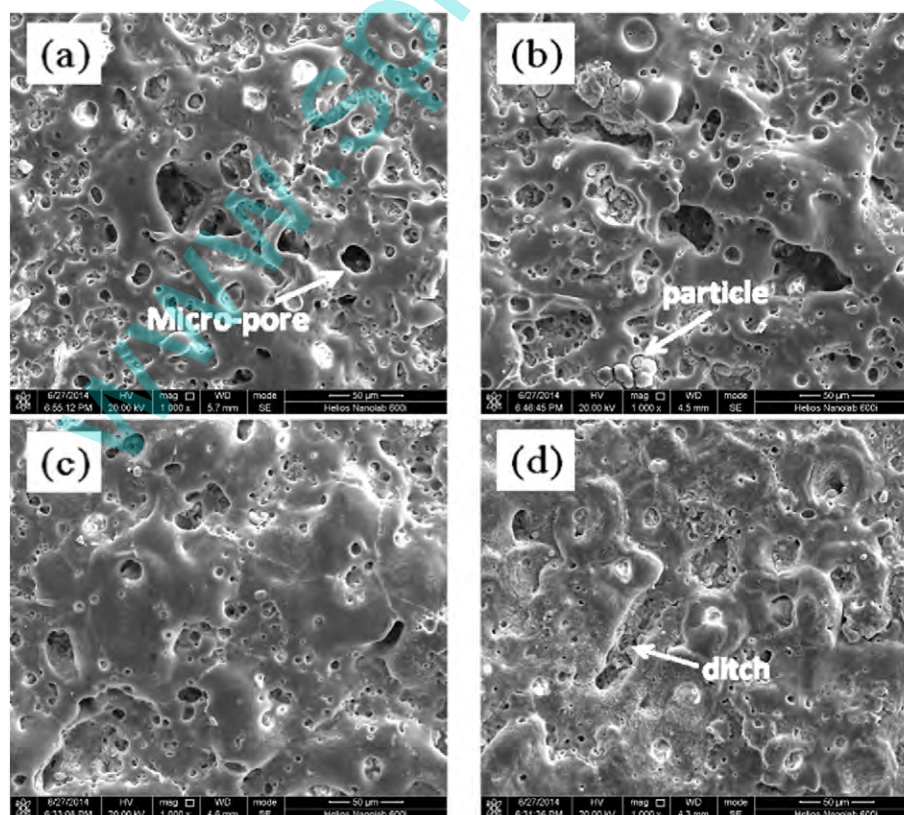


Fig. 1. Surface images of PEO coatings prepared under different concentrations of  $Zr(NO_3)_4$ : (a) 0 g/L; (b) 5 g/L; (c) 10 g/L; and (d) 15 g/L.

### 2.3. Thermal control property of the PEO coatings

The emittance of coatings was measured using a portable solar absorption/reflectorometer (TEMP 2000A, US) at 300 K, which also performs the measurement of the hemisphere reflectivity in the wavelength region from 3 to 35  $\mu\text{m}$ . The solar absorbance in the 0.2–2.5  $\mu\text{m}$  wavelength range was measured by an ultraviolet-visible-near infrared spectrophotometer (Perkin Elmer Lambda 950, US) equipped with a barium sulfate coated integrating sphere.

## 3. Results and discussion

### 3.1. Surface morphologies and element analysis of PEO coatings

The colors of the prepared PEO coatings are white or gray white from the visual observation. Fig. 1 shows the surface microstructure of the PEO coatings prepared under different  $\text{Zr}(\text{NO}_3)_4$  concentrations. Obviously, it can be observed that many micro-pores with different sizes and shapes distributed on the surface of coatings randomly. The size and number of pore decreased with the increase of the  $\text{Zr}(\text{NO}_3)_4$  concentrations. The porous structure is one typical characteristic of the PEO coating and composed of the metal oxide ceramic. During the PEO process, the micro discharge channels with high temperature and high pressure was generated by the advanced high-voltage anodizing on the substrate, along with the appearance of a mass of sparks and

gas bubbles [31]. Vigorous anodic oxidation reaction made the metal surface melting to form the molten oxide, which was thrown out of channels and then rapidly solidified by the surrounding cooling electrolyte. Thus, the nature of pore formation was attributed to the existence of micro discharge channels.

Besides, the microstructure was also affected by the acid and alkaline of electrolyte for the same substrate. As shown in Fig. 1b and d, there were some particles and ditches related to the variation of  $\text{H}^+$ , which accelerated the solution to erode the coating to greatly influence its roughness and thickness. While the concentration of  $\text{Zr}(\text{NO}_3)_4$  was 10 g/L, the electrolyte PH was suitable for the formation of the coating on AZ31 Mg alloy. In order to further investigate the reaction mechanism of the PEO coating shown in Fig. 1c, the corresponding surface elemental content and distribution analysis of the coating were shown in Fig. 2.

As is seen from scanning maps (Fig. 2a), there were Mg, O, Zr, Na, P and K elements uniformly distributed on the coating surface. EDS analysis of the coating revealed the percent content of elements in detail (Fig. 2b), and again demonstrated that these elements were introduced into the coating structure during the PEO process. Clearly, Mg element in the substrate was incorporated into the coating, yet others mainly from the electrolyte. The presence of Na and K elements in the coating probably involves two reasons: (i) the principle of electric neutrality [25] and (ii) the adsorption of the phosphate [39,40]. It was confirmed that ions in the electrolyte penetrated into discharge channels under

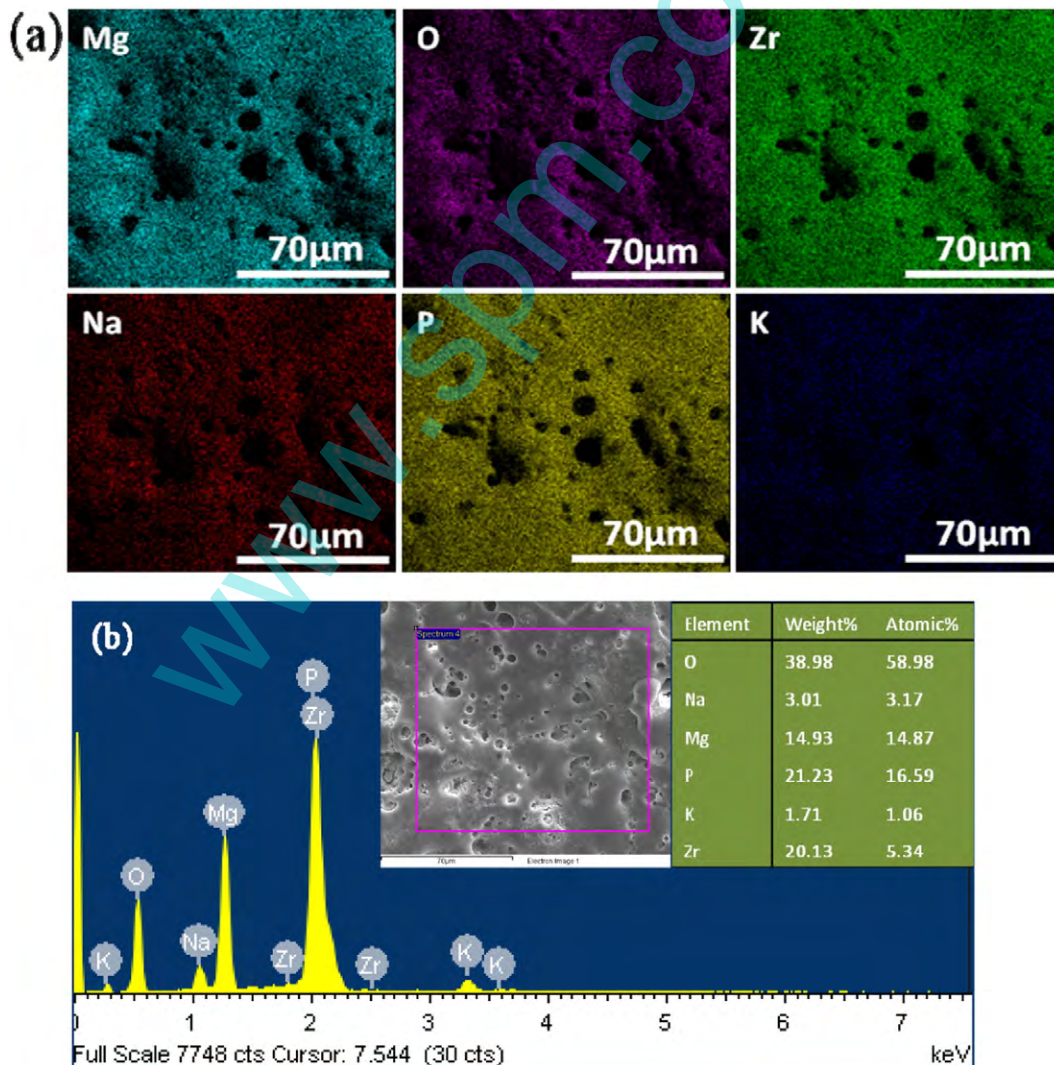


Fig. 2. Element compositions of the PEO coating prepared in the electrolyte with 10 g/L  $\text{Zr}(\text{NO}_3)_4$ : (a) surface scanning maps; (b) EDS analysis.

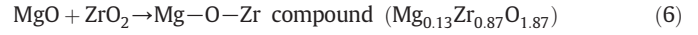
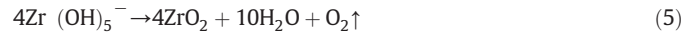
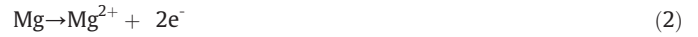
the effect of electric field and participated in the reaction process of the coating formation.

### 3.2. Cross-section morphologies and element distribution of PEO coatings

The cross-section microstructure of the PEO coatings prepared under different  $Zr(NO_3)_4$  concentrations are shown in Fig. 3. It was apparently found that all coatings were composed of transition layer and outer layer. The transition layer was compact and yet the outer layer was loose. Obviously, many micro-porous were formed in the outer layer due to the existence of micro discharge channels. On the contrast, the transition layer and the substrate were integrated metallurgically that is the representative characteristic of the PEO coating [33]. Additionally, some disconnected cracks in the coating were generated due to the existence of the unbalanced thermal-stress field in the PEO process [41].

The thickness and roughness of the coatings exhibit a dramatic change with the increase of the  $Zr(NO_3)_4$  concentration. Fig. 4 displays the AFM images of the PEO coatings obtained in the electrolytes with different  $Zr(NO_3)_4$  concentrations. The test results showed that the rms surface roughnesses with the increase of Zr ion concentration were 25 nm, 52.8 nm, 38.7 nm and 66 nm, respectively. Hence, when the concentration was 10 g/L, the thickness reached the maximum and the roughness was lower than those of other Zr-containing coatings. And it can be clearly seen from Fig. 3c that there were loss and small pores on the coating. Similar to the mechanism of the conventional anodic oxidation,  $Zr^{4+}$  ions can react with  $OH^-$  to form  $Zr(OH)_5^-$ , which will migrate from the electrolyte to the substrate interface and generate  $ZrO_2$  under high temperature and pressure. This reaction was

beneficial to accelerate the growth rate of coatings during the PEO process. The chemical equations related to the electrochemical reactions are given below:



However, the content level of  $Zr^{4+}$  ions could directly affect the alkaline–acid balance [42,43]. The  $Zr^{4+}$  ions could lead to the formation of  $Zr(OH)_5^-$ , which was beneficial to the growth of the coating. However, as the concentration of  $Zr(NO_3)_4$  increased, the alkaline–acid balance of the electrolyte would be destroyed, leading to the deposition of  $Zr(OH)_4$  and the increased concentration of  $H^+$  ions from the ionization of water, which would accelerate the erosion rate of the coating. As a result, the thickest coating could be obtained between 5 g/L and 15 g/L, in this paper, when the concentration of  $Zr(NO_3)_4$  was 10 g/L, the coating has the highest thickness. Besides, under this consideration, the spark discharge and electric breakdown would generate at the thin zone of the coating easily during the PEO reaction, where oxides were constantly produced to accelerate the growth rate of the coating and smooth the coating; thus the roughness was lowest. All the above showed that adding proper levels of Zr ion could increase the thickness of the coating

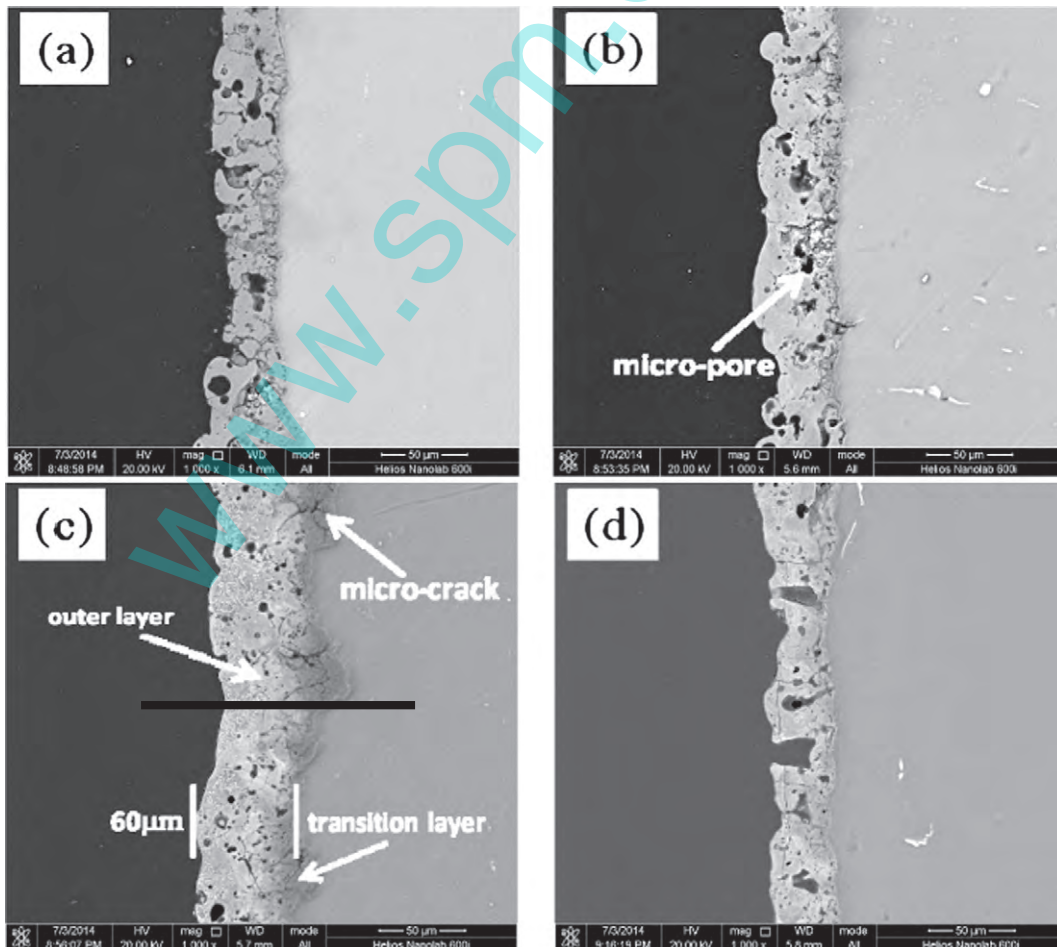


Fig. 3. Cross-section morphologies of PEO coatings formed under different concentrations of  $Zr(NO_3)_4$ .

and affect the roughness, which was consistent with the analysis results for the surface microstructure.

It has been known that Mg, O, Zr, Na, P and K elements were uniformly distributed on the surface (Fig. 2a). In order to deeply determine the tendency of the elementary distribution from the coating to the substrate (Fig. 3c), line scanning maps of Mg, O and Zr elements were examined by EDS analysis as shown in Fig. 5. The presence of such continuous element distribution at the transition layer demonstrated that the existence of the tight physic-chemical bonding mostly composed of Mg–O, Zr–O and Mg–O–Zr, which can improve the adherence of the coating [33,44,45]. And the pull-off test proved that all bonding strengths of the obtained coatings were higher than 10 MPa. Both Mg and O content were enhanced in the transition layer, which was corresponding with the PEO method and also explained that Mg in the coating mostly came from the substrate. The tendency of Zr element profile demonstrated that Zr element from the electrolyte mainly enriched in the outside layer. Presumably, the continuity trend of element distribution possibly indicated that the coating was mostly composed of Mg–O–Zr compounds which may enhance the bond strength of coating.

### 3.3. Phase and chemical composition of PEO coatings

In order to thoroughly ascertain the phase composition of PEO coatings prepared under different concentrations of Zr (NO<sub>3</sub>)<sub>4</sub>, the compounds on the coating after the PEO process were evaluated by XRD analysis, as shown in Fig. 6. It can be obtained that the PEO coating was mainly composed of Mg, MgO, t-ZrO<sub>2</sub> and an Mg–O–Zr compound (Mg<sub>0.13</sub>Zr<sub>0.87</sub>O<sub>1.87</sub>) by comparing with the ASTM cards. Mg diffraction peaks had a high intensity due to the porous structure or/and the relatively thin zones on the coating, which easily provided an accessible pathway for X-ray to reach the inside substrate [46]. Thus the thicker

the coatings, the weaker the intensity of the peaks from the Mg alloy substrate. During the advanced high-voltage PEO process, Mg and Zr ions were involved in the oxidation reaction to respectively produce MgO and the stable phase t-ZrO<sub>2</sub>. The two oxides were melted in the micro discharge channels and then rapidly cooled to form the Mg–O–Zr ceramic compound. It could be apparently found that the diffraction intensity of t-ZrO<sub>2</sub> and the Mg–O–Zr compound peaks significantly strengthened with the increase of Zr<sup>4+</sup> ion concentration. In XRD patterns, the crystal planes of t-ZrO<sub>2</sub> peaks corresponding to (011), (110), (020) and (121) were matched with the 50-1089# ASTM card, and the Mg–O–Zr compound plane (111), (200), (220) and (311) corresponding with 54-1266#. Compared with the results of EDS analysis, there were no diffraction peaks corresponding to P elements which possibly existed as the amorphous phase in the coating [39,40,47,48].

Hence, the chemical composition of the PEO coatings was further characterized by XPS analysis. Fig. 7 shows the XPS results of the coating prepared with 10 g/L Zr (NO<sub>3</sub>)<sub>4</sub>. Note that the correction of all the binding energies was referenced to the electronic core level of C (1s) at 284.6 eV. Zr (3d) peak was divided into Zr (3d<sub>5/2</sub>) and Zr (3d<sub>3/2</sub>) sub-peaks by the method of XPS peak differentiating analysis as shown in Fig. 7a. The binding energies of two sub-peaks were respectively 182.7 eV and 185.0 eV, which was corresponding to the photoelectrons energy of Zr<sup>4+</sup> in ZrO<sub>2</sub> [49,50]. It was concluded that Zr ion in the electrolyte was deposited on the substrate under the force of electric field, and then formed ZrO<sub>2</sub> during the PEO process. Fig. 7b shows Mg (1s) core level at the binding energy of 1303.2 eV, demonstrating that the magnesium state was merely existed as the form of Mg<sup>2+</sup> [51]. However, it was known from the literature that the doublets of Zr (3d<sub>5/2</sub>) and Zr (3d<sub>3/2</sub>) levels for pure ZrO<sub>2</sub> were respectively located at 182.2 eV and 184.6 eV, yet Mg (1s) peak for pure MgO was located at 1303.6 eV [51,52]. Hence, the binding energy of Zr (3d) peak of the PEO coating

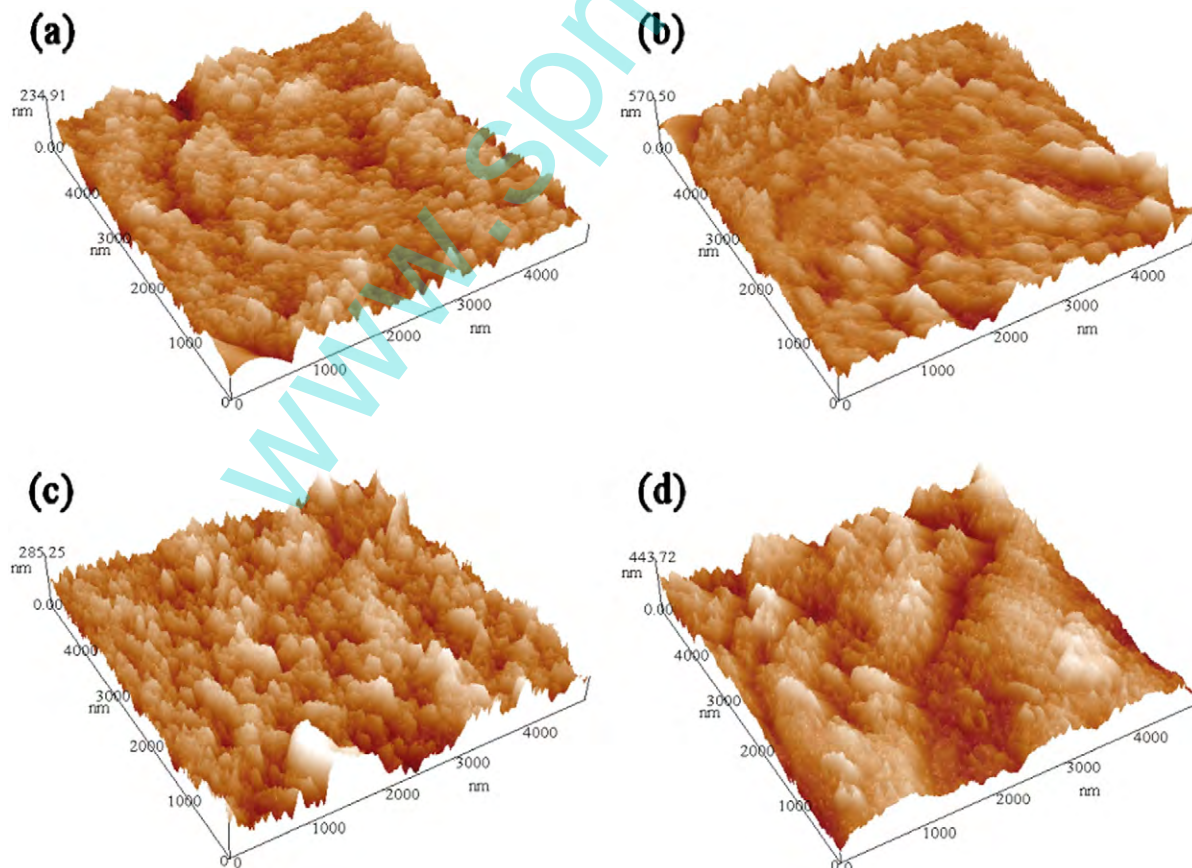


Fig. 4. AFM images of PEO coatings obtained in the electrolytes with different Zr(NO<sub>3</sub>)<sub>4</sub> concentrations: (a) 0 g/L; (b) 5 g/L; (c) 10 g/L; and (d) 15 g/L.

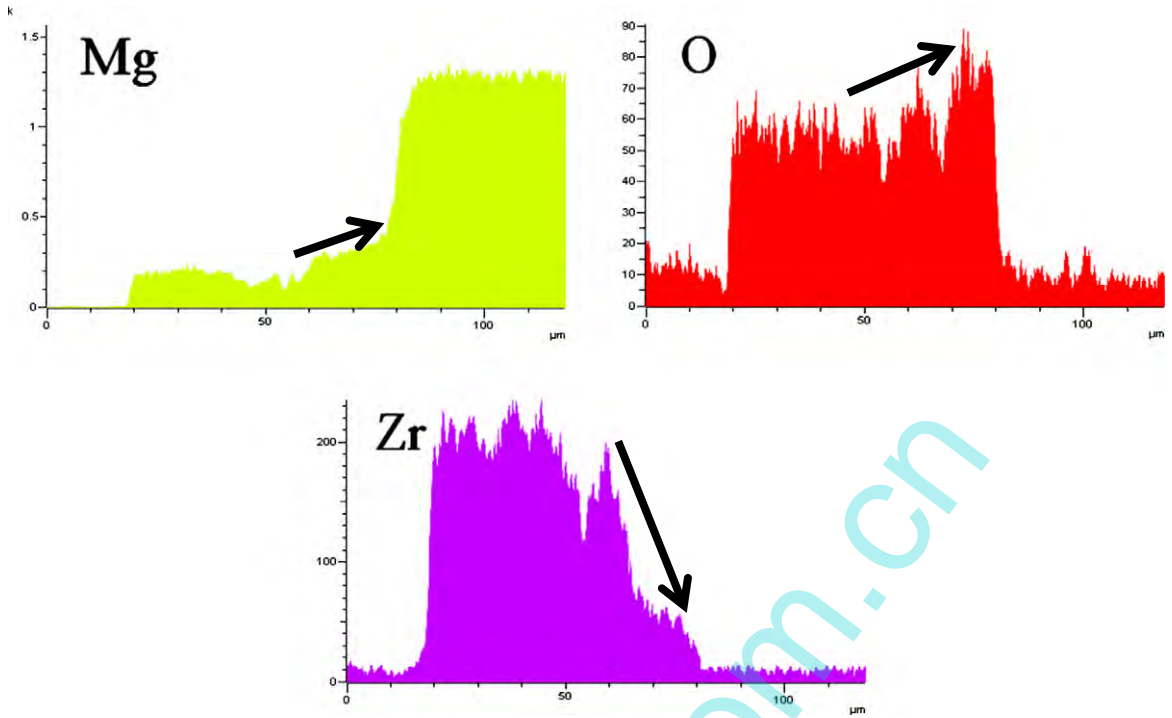


Fig. 5. EDS line scanning analysis corresponding to the black line shown in Fig. 3(c).

was higher and that of Mg (1 s) peak was lower, indicating that a chemical shift [52]. Due to the high magnesium content at the surface of the coating, chemical shifts of core level could arise. It was possible that

the charge-transfer of both Mg and Zr ions caused the charge redistribution between them. This could increase the average positive charge on the Zr ion and decrease that on the Mg ion, resulting in a higher binding

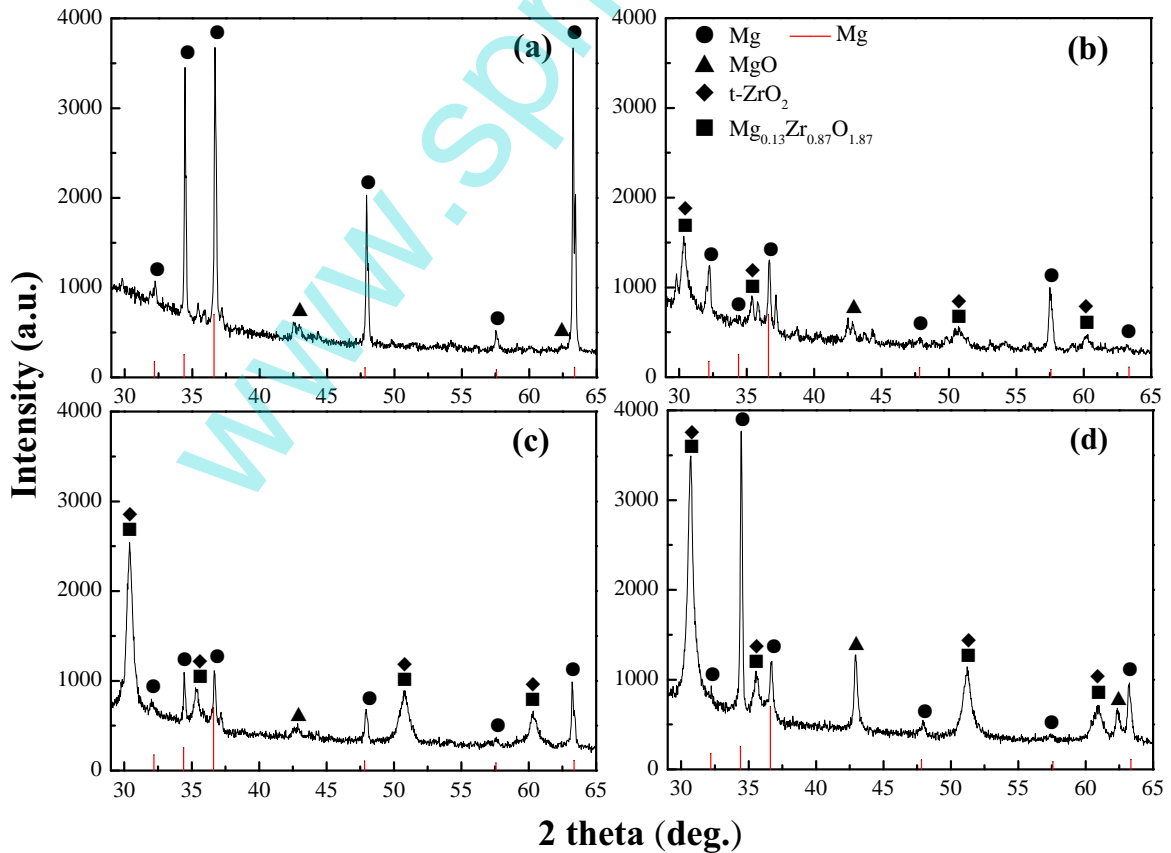


Fig. 6. XRD patterns of PEO coatings under different concentrations of  $Zr(NO_3)_4$ : (a) 0 g/L; (b) 5 g/L; (c) 10 g/L; and (d) 15 g/L.

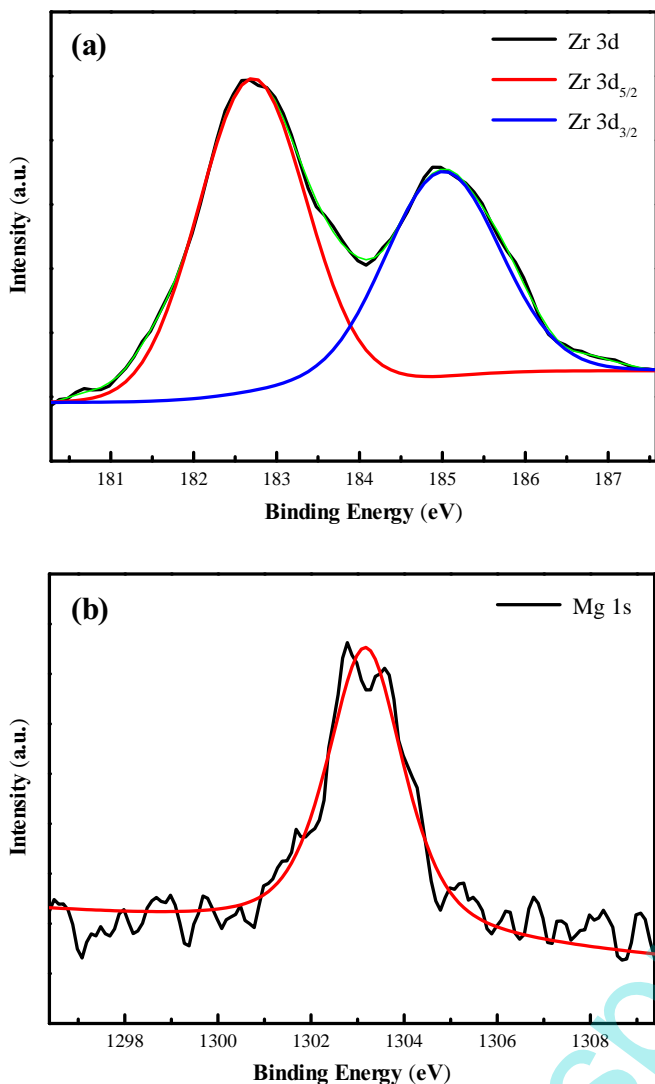


Fig. 7. XPS spectra of the PEO coating prepared in the electrolyte containing 10 g/L  $Zr(NO_3)_4$ : (a) Zr 3d peak; and (b) Mg 1s peak.

energy of the Zr (3d) peak. These results basically accorded with relevant reports and proved that the prepared coatings mainly were composed of the zirconium and magnesium oxide [53].

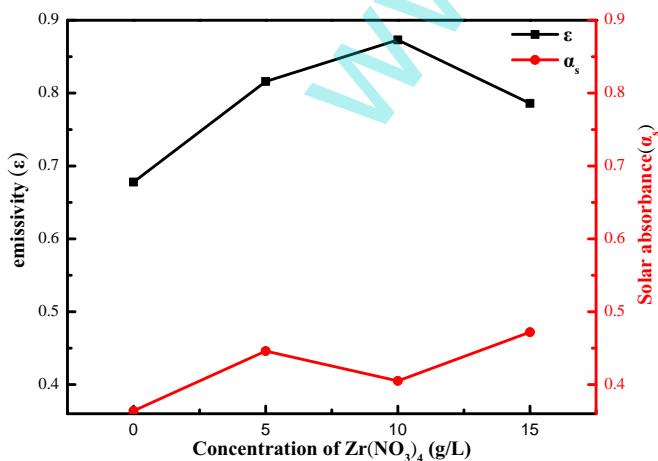


Fig. 8. Solar absorbance and emissivity of the PEO coatings prepared under different concentrations of  $Zr(NO_3)_4$ .

### 3.4. Thermal control characterization

As is known to us, the performance of thermal control coatings is controlled by the ratio of the solar absorbance ( $\alpha_s$ ) to the emissivity ( $\varepsilon$ ), namely  $\alpha_s/\varepsilon$ . The smaller the ratio, the better the thermal control effect is. Fig. 8 depicted the solar absorbance and emissivity variation of the PEO coatings with the increase of  $Zr^{4+}$  ion concentration. Compared with the coating prepared in the electrolyte without the  $Zr(NO_3)_4$  additives, the solar absorbance and emissivity of the coatings were generally increased with the adding of  $Zr^{4+}$  ions. It was indicated that the appropriate adding of  $Zr^{4+}$  ions in the electrolyte can effectively and notably improve the thermal control property of the PEO coating. Where, the emissivity value exhibited greater increases than that of the solar absorbance due to the existence of  $ZrO_2$  crystal structure in the coating. According with impact parameters of the thermal control properties, the ratio  $\alpha_s/\varepsilon$  value of the coating reached the minimum and about 0.46 when the concentration of  $Zr(NO_3)_4$  was 10 g/L. Concretely, under this concentration, the absorbance value was 0.405, and the emissivity one reached the maximum and was 0.873. As was shown in Fig. 3 (b–d), the emissivity was found to be increased with the increase of the coating thickness [54,55], but the decrease of the absorbance was related to the roughness.

The zirconium dioxide is a heat-resisting material (melting point about 2700 °C), which was usually used to prepare the thermal barrier coating due to its low thermal conductivity (about 4 W/(K m)). And the thermal expansion coefficient of  $ZrO_2$  is approximately equivalent to that of the metal. From the previous data,  $ZrO_2$  itself possesses a low absorbance value and high emissivity value [56,57]; hence it is also suitable to serve as the thermal control material. Besides, MgO formed during the PEO process maybe play a part to stabilize the phase transformation of  $ZrO_2$  [58]. Zr ions in the electrolyte entered into the MgO crystal structure and then were induced to steadily transform into the stable t- $ZrO_2$  phase state. Thus, owing to the entry of Zr with unsaturated d electronic orbit into the MgO crystal lattice, the lattice imperfection and distortion were caused and the lattice vibration modes were changed. The localized vibration mode was generated in the imperfection to cause the electron transition, and then the emissivity was enhanced.

The colors of the prepared coatings are white, which are determined by  $ZrO_2$  and MgO formed during the process. It was well known that white-painted surfaces more effectively retain the heat from the solar radiation inward the coating than surfaces of any other color. And the thermal conductivity of the coating was further reduced due to the presence of  $ZrO_2$ , which enhanced the thermal isolation property of the coating. Hence, the white coatings prepared in this work also belong to the thermal control coating with the low absorbance. In addition, the solar absorbance was in connection with the roughness of the coating as shown in Fig. 3 (b–d). For the surface with low roughness, the reflectivity was strengthened to further decrease the solar absorbance. The thermal control coating with a low ratio  $\alpha_s/\varepsilon$  obtained by the PEO technique is of great significance for the design level of the thermal control system on the spacecraft.

### 4. Conclusions

The low absorbance–emissivity ratio thermal control coatings were successfully prepared on AZ31 Mg alloy by the plasma electrolytic oxidation performed in the electrolytes with  $Zr(NO_3)_4$  additives. The PEO coating was mainly composed of Mg, MgO, t- $ZrO_2$  and an Mg–O–Zr compound ( $Mg_{0.13}Zr_{0.87}O_{1.87}$ ), along with the amorphous state of phosphorus. The thickness of the coating was largely affected by the  $Zr(NO_3)_4$  content. The emissivity was strengthened with the increase of the thickness, but the solar absorbance was related to the color and roughness of the coatings. When the concentration of  $Zr^{4+}$  ions in the electrolyte was 10 g/L, the thermal control property of the coating achieved the best protection effect that the absorbance–emissivity

ratio reached the minimum and about 0.46, namely the emissivity and solar absorbance value was 0.873 and 0.405 respectively. Under this condition, the thickness reached the maximum and about 60  $\mu\text{m}$ , yet the roughness was lower than those of other Zr-containing coatings. It is very promising that the white coatings with low solar absorbance and high emissivity are applied to the thermal control system of the spacecraft.

### Acknowledgment

The authors thank the financial support from the Nature Science Foundation of China (No. 51078101, 51173033), the Fundamental Research Funds for the Central Universities (No. HIT.BREIII.2012224, 201312), and the Space Debris Program (No. K0202210).

### References

- [1] C.D. Gu, J.S. Lian, J.G. He, Z.H. Jiang, Q. Jiang, *Surf. Coat. Technol.* 200 (2006) 5413–5418.
- [2] H.E. Friedrich, B.L. Mordike, *Magnesium Technology: Metallurgy, Design Data, Applications*, Springer, 2006.
- [3] A.A. Luo, *J. Magn. Alloy.* 1 (2013) 2–22.
- [4] C.E. Castano, M.J. O'Keefe, W.G. Fahrenholtz, *Surf. Coat. Technol.* 246 (2014) 77–84.
- [5] Z.W. Song, G. Yu, Z.H. Xie, B.N. Hu, X.M. He, X.Y. Zhang, *Surf. Coat. Technol.* 242 (2014) 83–91.
- [6] J. Sun, G. Wang, *Surf. Coat. Technol.* 254 (2014) 42–48.
- [7] S. Wijewardane, D.Y. Goswami, *Renew. Sust. Energ. Rev.* 16 (2012) 1863–1873.
- [8] D.A. Jaworske, *Thin Solid Films* 290–291 (1996) 278–282.
- [9] X.H. Wu, W. Qin, B. Cui, Z.H. Jiang, W.Q. Lu, W.D. He, *J. Mater. Process. Technol.* 200 (2008) 405–409.
- [10] J.A. Johnson, J.J. Heidenreich, R.A. Mantz, P.M. Baker, M.S. Donley, *Prog. Org. Coat.* 47 (2003) 432–442.
- [11] V. Baturkin, *Acta Astronaut.* 56 (2005) 161–170.
- [12] N. Kiamarsipour, R.S. Razavi, K. Ghani, *Dyes Pigments* 96 (2013) 403–406.
- [13] Y.G. Han, W. Ma, Y.M. Xuan, *Appl. Surf. Sci.* 282 (2013) 363–369.
- [14] A. Hendaoui, N. Émond, S. Dorval, M. Chaker, E. Haddad, *Sol. Energy Mater. Sol. Cells* 117 (2013) 494–498.
- [15] H. Xing, H.J. Zhao, Y. Zhang, Q.X. Zhang, *Acta Astronaut.* 71 (2012) 99–108.
- [16] L.Q. Wang, J.S. Zhou, J. Liang, J.M. Chen, *Appl. Surf. Sci.* 280 (2013) 151–155.
- [17] Y. Goueffon, L. Arurault, C. Mabru, C. Tonon, P. Guigue, *J. Mater. Process. Technol.* 209 (2009) 5145–5151.
- [18] Z.P. Yao, Q.X. Shen, A.X. Niu, B. Hu, Z.H. Jiang, *Surf. Coat. Technol.* 242 (2014) 146–151.
- [19] H. Pokhmurska, B. Wielage, T. Lampke, T. Grund, M. Student, N. Chervinska, *Surf. Coat. Technol.* 202 (2008) 4515–4524.
- [20] H. Hoche, J. Schmidt, S. Groß, T. Troßmann, C. Berger, *Surf. Coat. Technol.* 205 (2011) S145–S150.
- [21] X.M. Wang, L.Q. Zhu, H.C. Liu, W.P. Li, *Surf. Coat. Technol.* 202 (2008) 4210–4217.
- [22] T. Lei, C. Ouyang, W. Tang, L.F. Li, L.S. Zhou, *Surf. Coat. Technol.* 204 (2010) 3798–3803.
- [23] A.J. López, E. Otero, J. Rams, *Surf. Coat. Technol.* 205 (2010) 2375–2385.
- [24] R.O. Hussein, D.O. Northwood, X. Nie, *Surf. Coat. Technol.* 237 (2013) 357–368.
- [25] S. Stojadinović, M. Perić, J. Radić-Perić, R. Vasilčić, M. Petković, L. Zeković, *Surf. Coat. Technol.* 206 (2012) 2905–2913.
- [26] A.V. Timoshenko, Y.V. Magurova, *Surf. Coat. Technol.* 199 (2005) 135–140.
- [27] H. Tang, F.P. Wang, *Mater. Lett.* 93 (2013) 427–430.
- [28] D. Veys-Renaux, C.E. Barchiche, E. Rocca, *Surf. Coat. Technol.* 251 (2014) 232–238.
- [29] P.B. Su, X.H. Wu, Z.H. Jiang, *Mater. Lett.* 62 (2008) 3124–3126.
- [30] L. Wang, L. Chen, Z.C. Yan, W. Fu, *Surf. Coat. Technol.* 205 (2010) 1651–1658.
- [31] L.O. Snizhko, A.L. Yerokhin, N.L. Gurevina, V.A. Patalakha, A. Matthews, *Thin Solid Films* 516 (2007) 460–464.
- [32] J.A. Curran, T.W. Clyne, *Surf. Coat. Technol.* 199 (2005) 168–176.
- [33] R.O. Hussein, X. Nie, D.O. Northwood, *Electrochim. Acta* 112 (2013) 111–119.
- [34] A. Němcová, P. Skeldon, G.E. Thompson, B. Pacal, *Surf. Coat. Technol.* 232 (2013) 827–838.
- [35] Y.G. Ko, S. Namgung, D.H. Shin, *Surf. Coat. Technol.* 205 (2010) 2525–2531.
- [36] S.T. Lu, W. Qin, X.H. Wu, X.D. Wang, *Mater. Chem. Phys.* 135 (2012) 58–62.
- [37] M. Boinet, S. Verdier, S. Maximovitch, F. Dalard, *Surf. Coat. Technol.* 199 (2005) 141–149.
- [38] ISO 14916, *Thermal Spraying—Determination of Tensile Adhesive Strength*, 1999.
- [39] H.S. Ryu, W.H. Song, S.H. Hong, *Surf. Coat. Technol.* 202 (2008) 1853–1858.
- [40] A.L. Yerokhin, X. Nie, A. Leyland, A. Matthews, S.J. Dowey, *Surf. Coat. Technol.* 122 (1999) 73–93.
- [41] S. Durdu, M. Usta, *Appl. Surf. Sci.* 261 (2012) 774–782.
- [42] V.P. Tolstoy, B. Altangerel, *Mater. Lett.* 61 (2007) 123–125.
- [43] L. Wang, L. Chen, Z.C. Yan, H.L. Wang, J.Z. Peng, *J. Alloys Compd.* 493 (2010) 445–452.
- [44] A.A. Voevodin, A.L. Yerokhin, V.V. Lyubimov, M.S. Donley, J.S. Zabinski, *Surf. Coat. Technol.* 86–87 (1996) 516–521.
- [45] S.V. Gnedenkov, O.A. Khisanfova, A.G. Zavidnaya, S.L. Sinebrukhov, P.S. Gordienko, S. Iwatsubo, A. Matsui, *Surf. Coat. Technol.* 145 (2001) 146–151.
- [46] S.Y. Wang, Y.P. Xia, L. Liu, N.C. Si, *Ceram. Int.* 40 (2014) 93–99.
- [47] Z.P. Yao, B. Hu, Q.X. Shen, A.X. Niu, Z.H. Jiang, P.B. Su, P.F. Ju, *Surf. Coat. Technol.* 253 (2014) 166–170.
- [48] H. Tang, Q. Sun, T.Z. Xin, C.G. Yi, Z.H. Jiang, F.P. Wang, *Curr. Appl. Phys.* 12 (2012) 284–290.
- [49] J. Cerezo, P. Taheri, I. Vandendael, R. Posner, K. Lill, J.H.W. de Wit, J.M.C. Mol, H. Terryn, *Surf. Coat. Technol.* 254 (2014) 277–283.
- [50] X.L. Zhang, C.H. Wei, Y.Y. Song, X.P. Song, Z.B. Sun, *Int. J. Hydrog. Energy* 39 (2014) 15646–15655.
- [51] V.K. Mittal, S. Bera, R. Nithya, M.P. Srinivasan, S. Velmurugan, S.V. Narasimhan, *J. Nucl. Mater.* 335 (2004) 302–310.
- [52] W. Wang, H.T. Guo, J.P. Gao, X.H. Dong, Q.X. Qin, *J. Mater. Sci.* 35 (2000) 1495–1499.
- [53] F. Einkhah, K.M. Lee, M.A.F. Sani, B. Yoo, D.H. Shin, *Surf. Coat. Technol.* 238 (2014) 75–79.
- [54] M.M.S. Al Bosta, K.J. Ma, H.H. Chien, *Infrared Phys. Technol.* 60 (2013) 323–334.
- [55] S. Edalatpour, M. Francoeur, *J. Quant. Spectrosc. Radiat. Transf.* 118 (2013) 75–85.
- [56] Z.Y. Li, L.L. Yang, D.T. Ge, Y.B. Ding, L. Pan, J.P. Zhao, Y. Li, *Appl. Surf. Sci.* 259 (2012) 811–815.
- [57] G. Neuer, G. Jaroma-Weiland, *Int. J. Thermophys.* 19 (1998) 917–929.
- [58] O. Sarikaya, E. Celik, *Mater. Des.* 23 (2002) 645–650.